PAPER

Check for updates

Selective determination of Ag+ in the presence of Cd2+, Hg2+ and Cu2+ based on their different interactions with gold nanoclusters†

Rentian Guan, Lixia Tao, Yingying Hu, Cong Zhang, Yongping Wang, Min Hong [ID] and Qiaoli Yue [ID] *

In this work, a fluorescence method was developed for selective detection of Ag+ in the presence of Cd2+, Hg2+, and Cu2+ based on gold nanoclusters (AuNCs). That is, bovine serum albumin (BSA) templated AuNCs with double emission peaks were synthesized using BSA as a protective agent. AuNCs with uniform distribution and average size between 2.0 and 2.2 nm were synthesized using a green and simple method, and showed bright orange-red fluorescence under ultraviolet light. AuNCs have two emission peaks at 450 nm and 630 nm with an excitation wavelength of 365 nm. Under alkaline conditions, Cd^{2+} can combine with the surface sulfhydryl groups of BSA–AuNCs to form Cd–S bonds, which cause AuNCs to aggregate, resulting in an increase in fluorescence intensity at 630 nm. Conversely, due to the d^{10}–d^{10} metal affinity interaction, the addition of Hg^{2+} can reduce the fluorescence peak at 630 nm. Ag^+ was reduced to Ag^0 by gold nuclei in AuNCs, forming a stable hybrid Au@ AgNCs species with blue-shifted and enhanced fluorescence. Finally, the paramagnetic behavior of Cu^{2+} combined with BSA causes the excited electrons of the gold cluster to lose their energy via ISC, eventually leading to simultaneous quenching of the two emission peaks. The results show that the limit of detection (LOD) of Ag^+, Hg^{2+}, Cd^{2+} and Cu^{2+} is 1.19 μM, 3.39 μM, 1.83 μM and 5.95 μM, respectively.

Introduction

Metal nanoclusters (NCs), have been of great interest in nano-medicine for their use in biosensors,[1,2] bioimaging[2–4] and therapeutics.[5–7] Their ultra-small size (<2 nm) is ideal for drug delivery because it combines the advantages of low toxicity, high renal clearance and long blood circulation time.[5,6,8] Metal NCs consist of a few to about 100 atoms (usually gold (Au) or silver (Ag)) and differ from nanoparticles in that they exhibit molecular-like properties.[9–11] They have long-lived fluorescence in the infrared or near-infrared region and are excited by two light groups, which makes them very suitable for *in vitro* and *in vivo* imaging. Fluorescent metal (Au, Ag) nanoclusters (NCs) have become one of the most important nanomaterials, and have been widely used in sensing, biomarkers and biological imaging due to their excellent optical properties.[12–14]

Metal nanoclusters are very reactive in nature and tend to agglomerate without a protective base, and NCs are usually synthesized in solution by a fairly simple method using small organic molecules or polymers or biological templates.[9,15] Proteins are used as templates and reducers to construct stable

Department of Chemistry, Liaocheng University, Liaocheng 252059, China. E-mail: yueqiaoli@yahoo.com

† Electronic supplementary information (ESI) available. See DOI: 10.1039/d0ra05787h

and biocompatible metal nanoclusters.[16] Because the amines, carboxyls, and sulfhydryl groups in proteins can act as effective stabilizers for nanoparticles, proteins will play an important role in guiding the synthesis of functional nanomaterials under mild conditions.[17] BSA was selected for its biocompatibility, water solubility, affordability, and ubiquity in self-assembly, imaging, and sensor applications.[18–20] In addition, each BSA molecule has 28 cysteine and 20 tyrosine residues, resulting in greater capping and reduction capacity,[21,22] gold nano-clusters,[18,23] silver nanoclusters,[24] copper nanoclusters,[17,21] gold–silver bimetallic nanoclusters,[22] cerium–gold bimetallic nanoclusters,[25] and copper–zinc bimetallic nanoclusters[26] have been synthesized with BSA. In a paradigm-shifting work, Xie *et al.*[18] designed the first AuNCs for stable synthesis using BSA as a protein template. In recent years, the use of biological protein macromolecules (BSA,[18,24] lysozyme[27] and lactoferrin[28]) as stabilizers and reductants under alkaline conditions has been more popular.

Ag is widely used in jewelry, coins, medical, imaging, electrical and electronic equipment due to its excellent physical and chemical properties.[29,30] However, due to improper treatment of silver-containing products, Ag+ pollution has become a major environmental problem.[30] In addition, Ag+ has adverse effects on immune system, nervous system and digestive system.[31] In animal experiments, silver seemed to be distributed in all organs of the organisms studied, and the highest levels were

observed in the intestine and stomach.[28] Therefore, it is of great significance to construct a simple and rapid method with high sensitivity and selectivity to detect these metal ions.

Various methods have been used to detect Ag^+, including inductively coupled plasma mass spectrometry (ICP-MS),[31,32] atomic absorption spectroscopy (AAS),[33] and inductively coupled plasma emission spectroscopy (ICP-OES),[34] and these methods can be used well in lab. In the past few years, several optical sensors based on small organic molecules (fluorophores or chromophores),[35] biomolecules (proteins,[36] antibodies,[37] oligonucleotides,[38] and DNA enzymes[39]) and various polymer[40] and inorganic[41–45] materials have been developed for the detection of heavy metal ions. In addition, it will be attractive to develop a label-free approach with improved features such as cost, speed, simplicity, sensitivity, selectivity, compatibility with water based environments, and miniaturization.[46]

The focus of our work is to construct a novel approach to detect Ag^+ by using BSA as a template to synthesize AuNCs with double emission peaks. At the same time, it also has different response signals to Hg^{2+}, Cd^{2+} and Cu^{2+}. The experimental results show that the proposed method has a good sensitivity and selectivity for Ag^+ detection in the presence of Hg^{2+}, Cd^{2+} and Cu^{2+}.

Experimental

Materials and reagents

BSA was purchased from Sigma-Aldrich (St. Louis, MO, U.S.A.). The metal salts were ordered from Aladdin Reagent Co., Ltd. (Shanghai, China, http://www.aladdin-e.com). There were NaOH, $FeCl_3$, $CuCl_2$, $HgCl_2$, $Ho(NO_3)_3 \cdot 5H_2O$, $AgNO_3$, $ZnCl_2$, $Mn(CH_3COO)_2$, $MgCl_2$, $CrCl_3$, $Ce(NO_3)_3 \cdot 6H_2O$, $La(NO_3)_3 \cdot 6H_2O$, $Dy(NO_3)_3 \cdot 6H_2O$, $TbCl_3 \cdot 6H_2O$, $HAuCl_4 \cdot 3H_2O$, NaCl, $CdCl_2$, $CaCl_2$ and KCl. All chemicals from commercial sources were of analytical grade and used directly without further purification if no special instructions. All solutions were prepared and diluted by ultrapure water from Milli-Q water purified system.

Instruments

Fluorescence spectra and intensity were obtained on an F-7000 spectrophotometer (Hitachi, Japan, https://www.hitachi-hightech.com). Absorption spectral measurements were carried out on a UV-750 ultraviolet spectrophotometer (Perkin-Elmer, USA, http://yeepart.com). Transmission electron microscope (TEM) images were performed on a JEM 2100 electron microscope (JEOL Ltd., Japan, https://www.jeol.co.jp). TEM worked with an acceleration voltage at 200 kV, and a carbon-coated copper grid was used for sample suspension. X-ray photoelectron spectroscopy (XPS) measurements were undertaken with a K-Alpha spectrometer (Thermo Scientific Ltd., USA, http://www.thermofisher.com). Circular dichroism spectral measurements were carried out on J-810 CD circular dichroism (Jasco, Japan, http://www.jasco.co.jp). In addition to this, there are ZF-6 three-purpose ultraviolet analyzer (Jintan Shenglan Instrument Manufacturing Co., Ltd., China, https://www.czshenglan.com/), ultracentrifuge (Hitachi, Japan,

https://www.hitachi-hightech.com), DZ-2A vacuum drying oven (Tianjin Taisite Instrument Co., Ltd., http://www.taisite.cn/en_product-11.html), DF-101S collector type constant temperature heating magnetic stirrer, 12 kDa dialysis bag and ordinary carbon film copper mesh.

Synthesis of gold nanoclusters

Fluorescent BSA–AuNCs synthesized through BSA-mediated reduction of $HAuCl_4$ were based on a modification of a previously reported method.[18] Wash all glassware used for the experiment with aqua regia. 30 mL BSA solution with a concentration of 50 mg mL^{-1} was prepared in deionized water at room temperature (25 °C). To the solution was added 30 mL of $HAuCl_4$ (10 mM) under magnetic stirring. After two minutes, 1.0 M NaOH solution (5 mL) was added. The temperature was gradually raised to 60 °C, and the reaction was allowed to proceed under vigorous stirring 3 hours. The golden yellow solution gradually turned into a brown solution indicating the formation of red fluorescent AuNCs. After cooling to room temperature, the resulting AuNCs were dialyzed for 48 hours (water exchange every 12 hours) in a dialysis membrane having a molecular weight cut off of 12 kDa for purification. The as prepared BSA–AuNCs were stored at 4 °C for further use.

Detection procedure

Detection of metal ions was performed in aqueous solution at room temperature. First, standard stock solutions of Ag^+, Hg^{2+}, Cd^{2+}, Cu^{2+} with different concentrations were prepared by dissolving metal ions in deionized water. Subsequently, freshly prepared aliquots of AuNCs were added to 1.5 mL microcentrifuge tube and diluted twice. Then, different concentrations of different metal ion (Ag^+, Hg^{2+}, Cd^{2+}, Cu^{2+}) solutions were added and mixed solution in a vortex mixer. The fluorescence spectra of the resulting solutions was recorded (Ex = 360 nm). As can be seen from Scheme 1, AuNCs have dual emission peaks at 450 nm and 630 nm, respectively. When Ag^+ was added, the peak at 450 nm remained unchanged, and the peak at 630 nm blue-shifted. After Hg^{2+} was added, the peak at 450 nm remained unchanged, and the fluorescence intensity at 630 nm gradually decreased with the increase of Hg^{2+}. After adding Cu^{2+}, the fluorescence intensity at the peak of 450 nm and 630 nm decreased gradually with the increase of Cu^{2+}. After
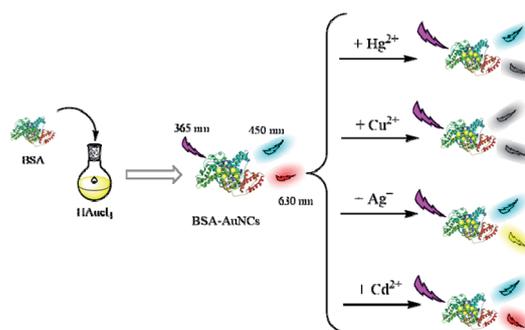
Scheme 1 Schematic diagram of AuNCs for detecting metal ions.

Cd^{2+} was added, the peak at 450 nm remained unchanged, and the fluorescence intensity at 630 nm increased with the increase of Cd^{2+}.

Results and discussion

Characterization of the AuNCs

The template synthesis process for AuNCs is shown in Scheme 1. As previously reported,[18] AuNCs templated by BSA were synthesized by a simple and environmentally friendly synthesis approach. TEM image (Fig. 1) showed that the obtained BSA functionalized AuNCs were monodisperse with an average size of 2.1 ± 0.38 nm and the size of 62% of the observed AuNCs distributed from 2.0 to 2.2 nm. HR-TEM image shows a lattice spacing of 2.33 Å (Fig. 1a, inset) that agrees well with the Au(111) facet.[47,48] As demonstrated in Fig. 2, XPS result for Au $4f_{7/2}$ can be deconvoluted into two components centered at Au^0 (83.7 eV) and Au^+ (87.7 eV), which is in good consistency with the previously reported AuNCs.[49] The circular dichroism spectra were measured by a circular dichroism chromatograph. In the far infrared region, the sample was analyzed in a well-cleaned quartz cuvette with a path length of 1 cm. The wavelength *versus* mdge values are plotted in Fig. S1.†

At the same time, we also studied the optical properties of AuNCs and discussed the UV-vis absorption spectra and fluorescence spectra of AuNCs. As seem in Fig. S2,† AuNCs exhibit bright red fluorescence under the illumination of a 365 nm UV lamp. The UV absorption is illustrated in Fig. 3. There is an
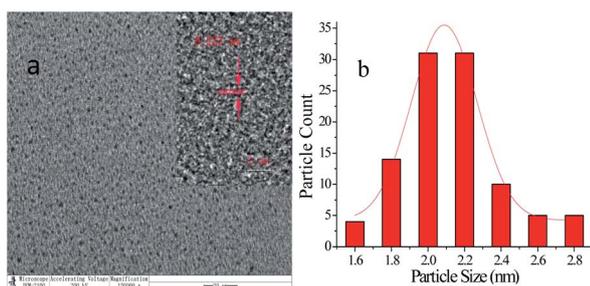

Fig. 1 TEM images (a) (inset, the HR-TEM images) and particle size distribution diagram (b) of AuNCs.
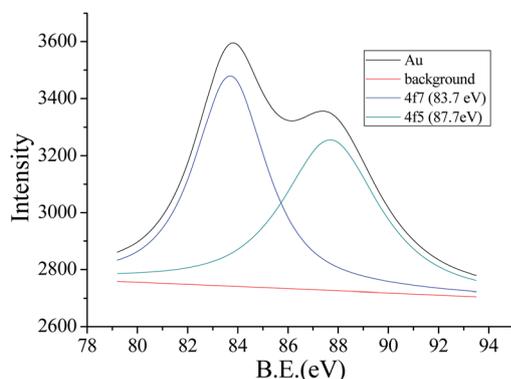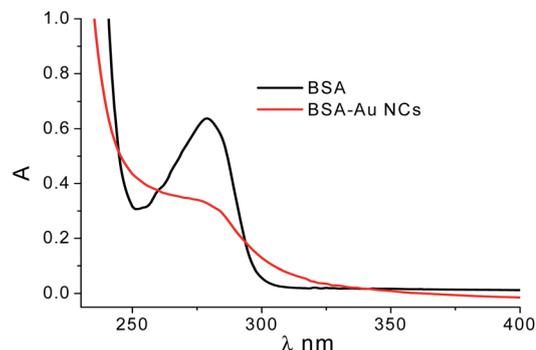

Fig. 2 XPS pattern of AuNCs.

Fig. 3 Ultraviolet absorption spectra of AuNCs and BSA.

absorption peak at 280 nm and a significant absorption peak at 360 nm, which is the optimal excitation wavelength of the fluorescence (emission peak at 450 nm and 630 nm). Using Rhodamine B as a reference, the relative quantum yield (QY) of AuNCs was calculated to be 3.36%, as shown in Fig. S3.†

Optimization of conditions

The influences of experimental conditions for metal ions assay were investigated in detail. It was carried out on buffer composition, ionic strength and pH for practical detection applications. The ultrapure water is used as detection media.

Effect of buffer species

We investigated the different buffer systems (10 mM) for testing the effects of metal ions, including NaH_2PO_4–Na_2HPO_4 solution, Tris–HCl solution, HEPES solution, NaAc–HAc solution and $Na_2B_2O_7$ solution. Five aliquots of freshly prepared AuNCs were diluted twice with the above five buffers and the fluorescence intensity was measured, as shown in Fig. S4.† By contrast, it is apparent from the figure that the HEPES buffer system has the largest change in fluorescence intensity, that is, the detection of metal ions in the HEPES buffer solution is the most sensitive compared to the five buffer systems. Therefore, the optimal buffer solution for the detection of various metal ions by AuNCs is the HEPES solution.

Effect of ionic strength

In this work, we used NaCl to adjust the ionic strength and explore the effect of NaCl concentration on the fluorescence intensity of AuNCs. The effect of NaCl concentration on the fluorescence intensity of AuNCs was measured using different concentrations of NaCl (including 0, 0.5, 1.0, 1.5 and 2.0 mM), as seen in Fig. S5.† It can be inferred that for the AuNCs products prepared by the experimental method, the fluorescence intensity does not change much in different ionic strength ranges, so it is concluded that the fluorescence stability of AuNCs is hardly affected by the ionic strength.

Effect of pH

The freshly prepared AuNCs were diluted twice with HEPES buffer and the pH of the whole system was adjusted to 5.5, 6.0,
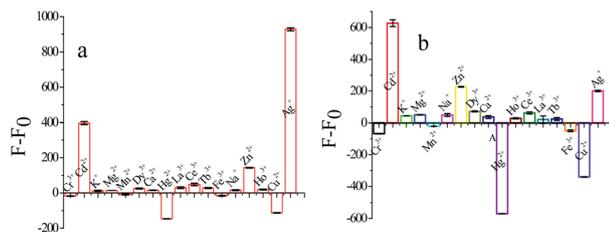
Fig. 4 Specificity of AuNCs for metal ions at 570 nm (a) and 630 nm (b).

6.5, 7.0, 7.5, 8.0, 8.5, 9.5 and 10.0 by adding an appropriate amount of NaOH or HCl. The fluorescence intensity of BSA–AuNCs at different pH values was measured, as shown in Fig. S6.† It can be observed from the figure that the fluorescence intensity of BSA–AuNCs at 450 nm increases gradually with the pH value, while the fluorescence intensity remains stable at 630 nm. In addition, comparing the fluorescence spectra of AuNCs after dialysis, it can be inferred that the pH of AuNCs after dialysis is weakly alkaline (pH 8 is measured after pH meter measurement) has no effect on metal ion detection.

Fluorescence lifetime detection

The fluorescence lifetime of BSA–AuNCs in the absence of Ag^+, Hg^{2+}, Cd^{2+}, Cu^{2+} and the presence of four metal ions was measured on an FL-TCSPC fluorescence spectrophotometer using the luminescence decay mode. The composite was excited by a 360 nm xenon flash and an emission wavelength of 630 nm and 570 nm, and then the fluorescence decay was recorded, as shown in Fig. S7 (Em = 630 nm) and Fig. S8† (Em = 570 nm).

Selectivity

Under optimal conditions, the selectivity of AuNCs was evaluated by adding 300 μM metal ions (Ag^+, Hg^{2+}, Cd^{2+}, Cu^{2+}) and detecting the response of AuNCs to other metal cations. A stock solution of various metal ions studied was prepared from metal salts. As illustrated in Fig. 4a, it can be observed that most of the metal ions at high concentrations cause only negligible fluorescence changes at 570 nm: Cr^{3+}, Mn^{2+}, Zn^{2+}, Dy^{3+}, Ho^+, La^{3+}, Tb^{3+}, Ce^{3+}, Ca^{2+}, Na^+, Mg^{2+}, K^+, and Fe^{3+} (5 times). The results confirmed that the determination of Ag^+ using the AuNCs

cluster system has good selectivity. At 630 nm, AuNCs also showed good selectivity in Hg^{2+}, $Cd^{2+}$and Cu^{2+} determination (Fig. 4b).

Sensitivity for metal ions detection

Four metal ions of Cd^{2+}, Ag^+, Hg^{2+} and Cu^{2+} were determined under the optimal conditions. The linear response of the fluorescence intensity to the concentration of Ag^+ is shown in Fig. 5. As the concentration of Ag^+ increases gradually, the peak at 450 nm remains unchanged and at 630 nm is blue-shift to 570 nm (Fig. 5a). The linear response of the fluorescence intensity to the concentration of Cd^{2+}, Hg^{2+} and Cu^{2+} are illustrated in Fig. S9.† When the concentration of Cd^{2+} increases, the peak at 450 nm remains unchanged, and the fluorescence intensity at 630 nm increases (Fig. S9a†). When the concentration of Hg^{2+} increases gradually, the peak at 450 nm also remains unchanged, and the fluorescence intensity at 630 nm decreases with the increase of Hg^{2+} (Fig. S9c†). When the concentration of Cu^{2+} increases, both the peaks of 450 nm and 630 nm decrease (Fig. S9e†). As shown in Fig. 5b, the fluorescence intensity of AuNCs shows a good linear response with Ag^+ concentration in the range of 5–400 μM with LOD of 1.19 μM. Meanwhile, the fluorescence intensity of AuNCs and the concentrations of Cd^{2+}, Hg^{2+} and Cu^{2+} also showed a good linear range of 10–100 μM (Fig. S9b†), 20–260 μM (Fig. S9d†), and 20–250 μM (Fig. S9f†) with the LOD at 1.83 μM, 3.39 μM, and 5.95 μM, respectively.

As shown in Table 1, the method in this paper was compared with the methods reported in the literature to analyze performance from material, linear range and detection limit. We
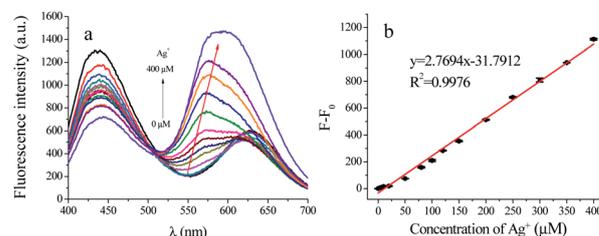

Fig. 5 Fluorescence spectra of AuNCs with the increase of Ag^+ concentration (a) and the linear response of fluorescence intensity of AuNCs at 570 nm to Ag^+ concentration (b).

Table 1 Comparison of the results for Ag^+ detection using different methods

| Method	Material	Linear range (μM)	LOD (μM)	Ref.
Fluorometry and colorimetry	Probe MNTPZ	0–100	1.36	50
Ratio fluorescence	Probe PPN	5–90	0.86	51
UV-vis spectral	Probe PTB-1	1.2–24	3.67	52
Electrochemistry	Fe_3O_4@Au nanoparticles and magnetic electrode	0.117–17.7	0.059	53
Colorimetry	Colorimetric sensor (DAC-Tu)	$10–1 \times 10^4$	10	54
Fluorometry and colorimetry	Probe L	0–30	1.7	55
Colorimetry	Paper-based colorimetric array test strip	—	1.69	56
Fluorometry	BSA–AuNCs	5–400	1.19	This work
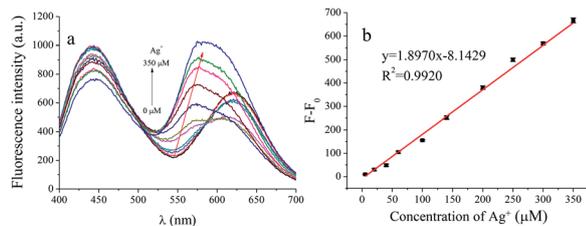
Fig. 6 The effects of Cu^{2+}, Hg^{2+} and Cd^{2+} (50 µM) on the detection of Ag^+ (a) and the linear response of fluorescence intensity of AuNCs at 570 nm to Ag^+ concentration (b).

found that the detection limit of this method was not the lowest, but the synthesis of AuNCs in this paper was simple in process, cheap in raw materials and convenient in operation.

In addition, we also detected the influence of Cu^{2+}, Hg^{2+} and Cd^{2+} (50 µM) on the detection of Ag^+. As shown in Fig. 6a, the peak at 630 nm is still blue-shift with the increase of Ag^+ concentration, and the peak intensity also increases gradually in the presence of Cu^{2+}, Hg^{2+} and Cd^{2+}. The linearity for Ag^+ detection in the mixture of Cu^{2+}, Hg^{2+} and Cd^{2+} (50 µM) are observed in Fig. 6b. It can be seen that Cu^{2+}, Hg^{2+} and Cd^{2+} have no obvious effect on the determination of Ag^+.

Based on the linear relationship between the fluorescence intensity of AuNCs and Ag^+ concentration, a fluorometric method was designed to detect Ag^+ rapidly. The test of Ag^+ detection was also carried out using solid substrate. After the silica gel plates were pretreated with AuNCs, a series of Ag^+ stock solutions prepared were dripped onto the plates in sequence. After the silica gel plate was dry, ultraviolet lamp was used to illuminate the silica gel plate at 365 nm, as shown in Fig. 7. The fluorescence intensity also increased gradually with the increase of Ag^+ concentration.

Analysis of real samples

Reliability of Ag^+ detection for the application in real samples was examined by recovery experiment using the standard addition method (Table 2). Lake water samples were collected from the artificial lake on campus of Liaocheng University. The recovery values range from 96.5% to 106.7% and the relative standard deviations (RSD) are from 1.59% to 2.76%. The above results reveal that the present fluorescent method can be applied to the analysis of Ag^+ in real samples.
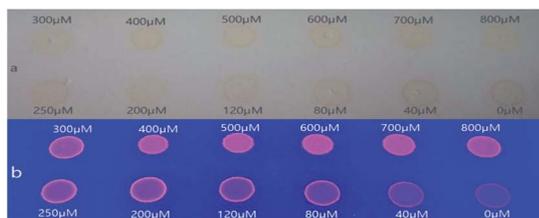

Fig. 7 Photographs of AuNCs in the presence of various concentrations of Ag^+ under the fluorescent lamp (a) and the ultraviolet lamp (b).

Table 2 The results of Ag^+ detection in lake water samples

Sample	Added µM	Found µM	Recovery%	RSD%
Lake water	20	19.3 ± 0.3	96.5	2.76
	50	49.2 ± 1.7	98.4	2.42
	100	106.5 ± 0.5	106.7	1.69
	200	213.8 ± 1.4	106.7	1.59
	250	260.1 ± 1.4	104.1	1.77

Possible mechanism

The newly designed dual emission biosensor was mainly based on the use of AuNCs as illustrated in Scheme 1.

As the concentration of Ag^+ increases, the fluorescence emission of BSA–AuNCs decreases slightly first, then blue shift occurs and increases at 570 nm. Once the blue shift in the emission spectrum occurs to 570 nm, even if the intensity gradually increases with the concentration of Ag^+, the emission peak does not shift further (Fig. 5a). Our synthetic dual-emitting AuNCs have a relatively small core size of BSA–AuNCs. Therefore, a similar response mechanism was proposed, The added Ag^+ were reduced to Ag^0 by gold nuclei in AuNCs, forming a stable Au@AgNCs hybrid species with blue-shifted and fluorescence enhancement, which deposited on the AuNCs surface inside the BSA, which remove surface defects of AuNCs and significantly increase AuNCs fluorescence intensity.[57–59]

It has been reported that Cd^{2+} can form Cd–SH complexes on AuNCs surface due to its interaction with sulfhydryl groups under alkaline conditions.[60,61] Therefore, in the presence of Cd^{2+}, the mechanism of AuNCs system fluorescence enhancement was hypothesized to be due to the formation of complexes between Cd^{2+} and BSA, which reduced the distance between AuNCs and resulted in aggregation and increased fluorescence intensity.[62]

It can be clearly observed from Fig. S9c† that with the gradual increase of Hg^{2+} concentration, the fluorescence intensity of double-emitting BSA–AuNCs does not change much at 450 nm, but the fluorescence intensity decreases sharply at 630 nm. Therefore, the most likely explanation for the quenching of BSA–AuNCs fluorescence, in the presence of Hg^{2+}, is based on the d^{10}–d^{10} metal affinity interaction between Au^+ and Hg^{2+} (Au^+–Hg^{2+}).[46,63,64]

It is a well-known fact that paramagnetic ions quench fluorescence by promoting ISC, thereby reducing fluorescence intensity. Therefore, the paramagnetic behavior of the combination of Cu^{2+} and BSA causes the excited electrons of the Au cluster to lose its energy as an ISC, resulting in quenching of fluorescence. With the increase of Cu^{2+} concentration, the fluorescence peaks at 450 nm and 630 nm are quenched (Fig. S9e†), confirming that quenching is achieved by Cu^{2+} binding to BSA rather than by free metal ions.[46]

Conclusions

In this work, we used BSA as a protective agent to synthesize gold nanoclusters with dual emission peaks (450 nm, 630 nm),

which can generate four different responses to four different metal ions, and can construct biosensing. When Cd^{2+} was added, the peak at 450 nm remained unchanged, and the fluorescence intensity at 630 nm peak increased with the increase of Cd^{2+}. After addition of Ag^+, the peak at 450 nm remained unchanged, and the peak at 630 nm blue-shifted. After adding Hg^{2+}, the peak at 450 nm remained unchanged, and the fluorescence intensity at 630 nm peak decreased with the increase of Hg^{2+}. After Cu^{2+} addition, the fluorescence intensity at the 450 nm and 630 nm peaks decreased with the increase of Cu^{2+}. The method has good selectivity and only responds to four metal ions of Cd^{2+}, Ag^+, Hg^{2+} and Cu^{2+}. This method is a viable tool for detecting metal ions and is of great significance for the research of biosensors.

Conflicts of interest

There are no conflicts to declare.

Acknowledgements

Notes and references

1 L. Zhang and E. Wang, Metal nanoclusters: new fluorescent probes for sensors and bioimaging, *Nano Today*, 2014, **9**, 132–157.

2 L. Y. Chen, C. W. Wang, Z. Yuan and H. T. Chang, Fluorescent gold nanoclusters: recent advances in sensing and imaging, *Anal. Chem.*, 2015, **87**, 216–229.

3 X. L. Guével, Recent advances on the synthesis of metal quantum-nanoclusters and their application for bioimaging, *IEEE J. Sel. Top. Quantum Electron.*, 2015, **20**, 45–56.

4 L. Shang, F. Stockmar, N. Azadfar and G. U. Nienhaus, Intracellular thermometry by using fluorescent gold nanoclusters, *Angew. Chem., Int. Ed. Engl.*, 2013, **52**, 11154–11157.

5 X. D. Zhang, J. Chen, Z. Luo, D. Wu, X. Shen, S. S. Song, Y. M. Sun, P. X. Liu, J. Zhao, S. Huo, S. Fan, F. Fan, X. J. Liang and J. Xie, Enhanced tumor accumulation of sub-2 nm gold nanoclusters for cancer radiation therapy, *Adv. Healthcare Mater.*, 2014, **3**, 133–141.

6 J. Liu, M. Yu, C. Zhou, S. Yang, X. Ning and J. Zheng, Passive tumor targeting of renal-clearable luminescent gold nanoparticles: long tumor retention and fast normal tissue clearance, *J. Am. Chem. Soc.*, 2013, **135**, 4978–4981.

7 T. D. Fernandez, J. R. Pearson, M. P. Leal, M. J. Torres, M. Blanca, C. Mayorga and X. Le Guevel, Intracellular accumulation and immunological properties of fluorescent gold nanoclusters in human dendritic cells, *Biomaterials*, 2015, **43**, 1–12.

8 X. D. Zhang, Z. Luo, J. Chen, X. Shen, S. Song, Y. Sun, S. Fan, F. Fan, D. T. Leong and J. Xie, Ultrasmall $Au_{10-12}(SG)_{10-12}$ nanomolecules for high tumor specificity and cancer radiotherapy, *Adv. Mater.*, 2014, **26**, 4565–4568.

9 J. Zheng, C. Zhou, M. Yu and J. Liu, Different sized luminescent gold nanoparticles, *Nanoscale*, 2012, **4**, 4073–4083.

10 R. Jin, Quantum sized, thiolate-protected gold nanoclusters, *Nanoscale*, 2010, **2**, 343–362.

11 D. E. Jiang, The expanding universe of thiolated gold nanoclusters and beyond, *Nanoscale*, 2013, **5**, 7149–7160.

12 Y.-H. Lin and W.-L. Tseng, Ultrasensitive sensing of Hg^{2+} and CH_3Hg^+ based on the fluorescence quenching of lysozyme type vi-stabilized gold nanoclusters, *Anal. Chem.*, 2010, **82**, 9194–9200.

13 M. Wang, Q. Mei, K. Zhang and Z. Zhang, Protein–gold nanoclusters for identification of amino acids by metal ions modulated ratiometric fluorescence, *Analyst*, 2012, **137**, 1618–1623.

14 Y. Yue, T. Y. Liu, H. W. Li, Z. Liu and Y. Wu, Microwave-assisted synthesis of BSA-protected small gold nanoclusters and their fluorescence-enhanced sensing of silver(I) ions, *Nanoscale*, 2012, **4**, 2251–2254.

15 L. Shang, S. Dong and G. U. Nienhaus, Ultra-small fluorescent metal nanoclusters: synthesis and biological applications, *Nano Today*, 2011, **6**, 401–418.

16 Y. Xu, J. Sherwood, Y. Qin, D. Crowley, M. Bonizzoni and Y. Bao, The role of protein characteristics in the formation and fluorescence of Au nanoclusters, *Nanoscale*, 2014, **6**, 1515–1524.

17 C. Wang, C. Wang, L. Xu, H. Cheng, Q. Lin and C. Zhang, Protein-directed synthesis of pH-responsive red fluorescent copper nanoclusters and their applications in cellular imaging and catalysis, *Nanoscale*, 2014, **6**, 1775–1781.

18 J. Xie, Y. Zheng and J. Y. Ying, Protein-directed synthesis of highly fluorescent gold nanoclusters, *J. Am. Chem. Soc.*, 2009, **131**, 888–889.

19 A. G. Tkachenko, H. Xie, D. Coleman, W. Glomm, J. Ryan, M. F. Anderson, S. Franzen and D. L. Feldheim, Multifunctional gold nanoparticle–peptide complexes for nuclear targeting, *J. Am. Chem. Soc.*, 2003, **125**, 4700–4701.

20 X. Chen and G. A. Baker, Cholesterol determination using protein-templated fluorescent gold nanocluster probes, *Analyst*, 2013, **138**, 7299–7302.

21 L. Xiaoqing, L. Ruiyi, L. Xiaohuan and L. Zaijun, Ultra sensitive and wide-range pH sensor based on the BSA-capped Cu nanoclusters fabricated by fast synthesis through the use of hydrogen peroxide additive, *RSC Adv.*, 2015, **5**, 48835–48841.

22 N. Zhang, Y. Si, Z. Sun, L. Chen, R. Li, Y. Qiao and H. Wang, Rapid, selective, and ultrasensitive fluorimetric analysis of mercury and copper levels in blood using bimetallic gold-silver nanoclusters with "silver effect"-enhanced red fluorescence, *Anal. Chem.*, 2014, **86**, 11714–11721.

23 C. Fu, C. Ding, X. Sun and A. Fu, Curcumin nanocapsules stabilized by bovine serum albumin-capped gold nanoclusters (BSA–AuNCs) for drug delivery and theranosis, *Mater. Sci. Eng., C*, 2018, **87**, 149–154.

24 C. Guo and J. Irudayaraj, Fluorescent Ag clusters *via* a protein-directed approach as a Hg(II) ion sensor, *Anal. Chem.*, 2011, **83**, 2883–2889.

25 Y. N. Chen, P. C. Chen, C. W. Wang, Y. S. Lin, C. M. Ou, L. C. Ho and H. T. Chang, One-pot synthesis of fluorescent BSA–Ce/Au nanoclusters as ratiometric pH probes, *Chem. Commun.*, 2014, **50**, 8571–8574.

26 H. Chen, L. Lin, H. Li, J. Li and J.-M. Lin, Aggregation-induced structure transition of protein-stabilized zinc/copper nanoclusters for amplified chemiluminescence, *ACS Nano*, 2015, **9**, 2173–2183.

27 H. Wei, Z. Wang, L. Yang, S. Tian, C. Hou and Y. Lu, Lysozyme-stabilized gold fluorescent cluster: synthesis and application as Hg^{2+} sensor, *Analyst*, 2010, **135**, 1406–1410.

28 C. Sun, H. Yang, Y. Yuan, X. Tian, L. Wang, Y. Guo, L. Xu, J. Lei, N. Gao, G. J. Anderson, X. J. Liang, C. Chen, Y. Zhao and G. Nie, Controlling assembly of paired gold clusters within apoferritin nanoreactor for *in vivo* kidney targeting and biomedical imaging, *J. Am. Chem. Soc.*, 2011, **133**, 8617–8624.

29 N. Hadrup and H. R. Lam, Oral toxicity of silver ions, silver nanoparticles and colloidal silver-a review, *Regul. Toxicol. Pharmacol.*, 2014, **68**, 1–7.

30 B. Li, X. Wang, X. Shen, W. Zhu, L. Xu and X. Zhou, Aggregation-induced emission from gold nanoclusters for use as a luminescence-enhanced nanosensor to detect trace amounts of silver ions, *J. Colloid Interface Sci.*, 2016, **467**, 90–96.

31 K. Ndung'u, M. A. Ranville, R. P. Franks and A. R. Flegal, On-line determination of silver in natural waters by inductively-coupled plasma mass spectrometry: influence of organic matter, *Mar. Chem.*, 2006, **98**, 109–120.

32 W. Guo, S. Hu, J. Zhang and H. Zhang, Elimination of oxide interferences and determination of ultra-trace silver in soils by ICP-MS with ion-molecule reactions, *Sci. Total Environ.*, 2011, **409**, 2981–2986.

33 C. Bianco, S. Kezic, M. Crosera, V. Svetlicic, S. Segota, G. Maina, C. Romano, F. Larese and G. Adami, *In vitro* percutaneous penetration and characterization of silver from silver-containing textiles, *Int. J. Nanomed.*, 2015, **10**, 1899–1908.

34 X. J. Yang, R. Foley and G. K. C. Low, A modified digestion procedure for analysing silver in environmental water samples, *Analyst*, 2002, **127**, 315–318.

35 E. M. Nolan and S. J. Lippard, Tools and tactics for the optical detection of mercuric ion, *Chem. Rev.*, 2008, **108**, 3443–3480.

36 S. V. Wegner, A. Okesli, P. Chen and C. He, Design of an emission ratiometric biosensor from MerR family proteins: a sensitive and selective sensor for Hg^{2+}, *J. Am. Chem. Soc.*, 2007, **129**, 3474–3475.

37 M. Matsushita, M. M. Meijler, P. Wirsching, R. A. Lerner and K. D. Janda, A blue fluorescent antibody-cofactor sensor for mercury, *Org. Lett.*, 2005, **7**, 4943–4946.

38 J. Greeley, W. P. Krekelberg and M. Mavrikakis, Strain-induced formation of subsurface species in transition metals, *Angew. Chem.*, 2004, **116**, 4396–4400.

39 J. M. Thomas, R. Ting and D. M. Perrin, High affinity DNAzyme-based ligands for transition metal cations – a prototype sensor for Hg^{2+}, *Org. Biomol. Chem.*, 2004, **2**, 307–312.

40 I.-B. Kim and U. H. F. Bunz, Modulating the sensory response of a conjugated polymer by proteins: an agglutination assay for mercury ions in water, *J. Am. Chem. Soc.*, 2006, **128**, 2818–2819.

41 J. S. Lee, M. S. Han and C. A. Mirkin, Colorimetric detection of mercuric ion Hg^{2+} in aqueous media using DNA-functionalized gold nanoparticles, *Angew. Chem., Int. Ed. Engl.*, 2007, **46**, 4093–4096.

42 X. Xue, F. Wang and X. Liu, One-step, room temperature, colorimetric detection of mercury Hg^{2+} using DNA/nanoparticle conjugates, *J. Am. Chem. Soc.*, 2008, **130**, 3244–3245.

43 G. K. Darbha, A. K. Singh, U. S. Rai, E. Yu, H. Yu and P. Chandra Ray, Selective detection of mercury(II) ion using nonlinear optical properties of gold nanoparticles, *J. Am. Chem. Soc.*, 2008, **130**, 8038–8043.

44 D. Li, A. Wieckowska and I. Willner, Optical analysis of Hg^{2+} ions by oligonucleotide-gold-nanoparticle hybrids and DNA-based machines, *Angew. Chem., Int. Ed. Engl.*, 2008, **47**, 3927–3931.

45 M. Rex, F. E. Hernandez and A. D. Campiglia, Pushing the limits of mercury sensors with gold nanorods, *Anal. Chem.*, 2006, **78**, 445–451.

46 J. Xie, Y. Zheng and J. Y. Ying, Highly selective and ultrasensitive detection of Hg^{2+} based on fluorescence quenching of Au nanoclusters by Hg^{2+}–Au^{+} interactions, *Chem. Commun.*, 2010, **46**, 961–963.

47 M. I. Halawa, B. S. Li and G. Xu, Novel synthesis of thiolated gold nanoclusters induced by lanthanides for ultrasensitive and luminescent detection of the potential anthrax spores' biomarker, *ACS Appl. Mater. Interfaces*, 2020, **12**, 32888–32897.

48 E. Ju, Z. Liu, Y. Du, Y. Tao, J. Ren and X. Qu, Heterogeneous assembled nanocomplexes for ratiometric detection of highly reactive oxygen species *in vitro* and *in vivo*, *ACS Nano*, 2014, **8**, 6014–6023.

49 M. Zhuang, C. Ding, A. Zhu and Y. Tian, Ratiometric fluorescence probe for monitoring hydroxyl radical in live cells based on gold nanoclusters, *Anal. Chem.*, 2014, **86**, 1829–1836.

50 P. R. Dongare, A. H. Gore, G. B. Kolekar and B. D. Ajalkar, A phenazine based colorimetric and fluorescent chemosensor for sequential detection of Ag^{+} and I^{-} in aqueous media, *Luminescence*, 2020, **35**, 231–242.

51 Q. Jiang, Z. Wang, M. Li, J. Song, Y. Yang, X. Xu, H. Xu and S. Wang, A nopinone based multi-functional probe for

colorimetric detection of Cu^{2+} and ratiometric detection of Ag^+, *Photochem. Photobiol. Sci.*, 2020, **19**, 49–55.

52 J. P. Nandre, S. R. Patil, S. K. Sahoo, C. P. Pradeep, A. Churakov, F. Yu, L. Chen, C. Redshaw, A. A. Patil and U. D. Patil, A chemosensor for micro- to nano-molar detection of Ag^+ and Hg^{2+} ions in pure aqueous media and its applications in cell imaging, *Dalton Trans.*, 2017, **46**, 14201–14209.

53 H. Yang, X. Liu, R. Fei and Y. Hu, Sensitive and selective detection of Ag^+ in aqueous solutions using Fe_3O_4@Au nanoparticles as smart electrochemical nanosensors, *Talanta*, 2013, **116**, 548–553.

54 L. Wang, C. Zhang, H. He, H. Zhu, W. Guo, S. Zhou, S. Wang, J. R. Zhao and J. Zhang, Cellulose-based colorimetric sensor with N, S sites for Ag^+ detection, *Int. J. Biol. Macromol.*, 2020, **163**, 593–602.

55 M. Sahu, A. Kumar Manna, K. Rout, J. Mondal and G. K. Patra, A highly selective thiosemicarbazone based Schiff base chemosensor for colorimetric detection of Cu^{2+} and Ag^+ ions and turn-on fluorometric detection of Ag^+ ions, *Inorg. Chim. Acta*, 2020, **508**, 119633.

56 L. Liu and H. Lin, Paper-based colorimetric array test strip for selective and semiquantitative multi-ion analysis: simultaneous detection of Hg^{2+}, Ag^+, and Cu^{2+}, *Anal. Chem.*, 2014, **86**, 8829–8834.

57 H. Liu, X. Zhang, X. Wu, L. Jiang, C. Burda and J. J. Zhu, Rapid sonochemical synthesis of highly luminescent non-

toxic AuNCs and Au@AgNCs and Cu (II) sensing, *Chem. Commun.*, 2011, **47**, 4237–4239.

58 C.-C. Huang, H.-Y. Liao, Y.-C. Shiang, Z.-H. Lin, Z. Yang and H.-T. Chang, Synthesis of wavelength-tunable luminescent gold and gold/silver nanodots, *J. Mater. Chem.*, 2009, **19**, 755–759.

59 H.-W. Li, Y. Yue, T.-Y. Liu, D. Li and Y. Wu, Fluorescence-enhanced sensing mechanism of BSA-protected small gold-nanoclusters to silver(I) ions in aqueous solutions, *J. Phys. Chem. C*, 2013, **117**, 16159–16165.

60 P. Huang, S. Li, N. Gao and F. Wu, Toward selective, sensitive, and discriminative detection of Hg^{2+} and Cd^{2+} *via* pH-modulated surface chemistry of glutathione-capped gold nanoclusters, *Analyst*, 2015, **140**, 7313–7321.

61 E. Chow, D. B. Hibbert and J. J. Gooding, Voltammetric detection of cadmium ions at glutathione-modified gold electrodes, *Analyst*, 2005, **130**, 831–837.

62 F. Mo, Z. Ma, T. Wu, M. Liu, Y. Zhang, H. Li and S. Yao, Holey reduced graphene oxide inducing sensitivity enhanced detection nanoplatform for cadmium ions based on glutathione–gold nanocluster, *Sens. Actuators, B*, 2019, **281**, 486–492.

63 S.-N. Ding and Y.-X. Guo, One-pot synthesis of dual-emitting BSA–Pt–Au bimetallic nanoclusters for fluorescence ratiometric detection of mercury ions and cysteine, *Anal. Methods*, 2015, **7**, 5787–5793.

64 P. Pyykko, Theoretical chemistry of gold, *Angew. Chem., Int. Ed. Engl.*, 2004, **43**, 4412–4456.